Bipedal Locomotion in Crawling Cells

Erin L. Barnhart,[†‡] Greg M. Allen,[†‡] Frank Jülicher,[§] and Julie A. Theriot[†‡¶*]
[†]Department of Biochemistry, Stanford University School of Medicine, Stanford, California; [‡]Howard Hughes Medical Institute, Stanford University School of Medicine, Stanford, California; [§]Max Planck Institute for the Physics of Complex Systems, Dresden, Germany; and [¶]Department of Microbiology and Immunology, Stanford University School of Medicine, Stanford, California

ABSTRACT Many complex cellular processes from mitosis to cell motility depend on the ability of the cytoskeleton to generate force. Force-generating systems that act on elastic cytoskeletal elements are prone to oscillating instabilities. In this work, we have measured spontaneous shape and movement oscillations in motile fish epithelial keratocytes. In persistently polarized, fan-shaped cells, retraction of the trailing edge on one side of the cell body is out of phase with retraction on the other side, resulting in periodic lateral oscillation of the cell body. We present a physical description of keratocyte oscillation in which periodic retraction of the trailing edge is the result of elastic coupling with the leading edge. Consistent with the predictions of this model, the observed frequency of oscillation correlates with cell speed. In addition, decreasing the strength of adhesion to the substrate reduces the elastic force required for retraction, causing cells to oscillate with higher frequency at relatively lower speeds. These results demonstrate that simple elastic coupling between movement at the front of the cell and movement at the rear can generate large-scale mechanical integration of cell behavior.

INTRODUCTION

Cell migration requires temporal and spatial integration of multiple force-generating systems (1–3). At the front of the cell, actin polymerization drives protrusion of the leading edge (4–6), and at the rear, actin depolymerization and myosin contraction facilitate retraction of the trailing edge and translocation of the cell body (7). Contractile forces generated by myosin II activity and by turnover of the elastic actin network are balanced by adhesions between the cell and the underlying substrate, enabling generation of traction force and net forward movement (3,8–11). Each of these processes—polymerization and depolymerization of the actin meshwork, myosin contraction, and adhesion—are complex, highly-regulated processes that have been well characterized individually, but the molecular and mechanical mechanisms that couple protrusion of the leading edge with retraction of the trailing edge are not well understood.

Fish epithelial keratocytes are notoriously well coordinated cells; in many keratocytes, protrusion of the leading edge is so tightly coupled with retraction of the trailing edge that migrating cells appear to glide across the substrate while maintaining a constant shape and speed (12). Recently, however, careful quantification of cell shape has shown that keratocytes from primary fish skin cultures are heterogeneous (13–15). Stereotypical, ''coherent'' keratocytes are fast-moving and fan-shaped, with smooth leading edges, whereas ''decoherent'' cells, in which protrusion and retraction are more loosely coupled, are rounder, slower-moving, and have a rough leading-edge morphology (13,14). Moreover, coherent keratocytes are directionally persistent, moving in one direction over many cell lengths of movement, whereas decoherent keratocytes tend to move in curved trajectories (13), suggesting that the protrusive, contractile, and adhesive forces required for migration are more tightly balanced in coherent keratocytes than in decoherent keratocytes.

The dynamic organization and mechanics of the keratocyte cytoskeleton have been extensively characterized, particularly in coherent keratocytes (2). Keratocytes have a broad, flat lamellipodium that consists of a densely branched actin meshwork (16). In coherent keratocytes, the anticapping protein Ena/VASP and filamentous actin are both enriched in the front center of the leading edge (13,14), and AFM measurements indicate that the elastic lamellipodium is stiffest near the front (17). The actin meshwork is organized with barbed ends primarily oriented toward the leading edge (16) and polymerization of the actin meshwork is tightly coupled to protrusion of the leading edge; photoactivation experiments and quantitative fluorescent speckle microscopy have demonstrated that the actin network is nearly stationary with respect to the underlying substrate (4,18). Adhesion proteins such as integrin and talin localize to the leading edge in fan-shaped keratocytes (19), and local disruption of adhesions with forces too small to stall actin polymerization nonetheless stall protrusion of the leading edge (20). In the rear of the cell, myosin contraction exerts force on the substrate perpendicular to the direction of cell movement (10,11,21), and these contractile forces are balanced by large adhesions on either side of the cell body (19,22). In decoherent cells, the cytoskeleton is less well organized, with no enrichment of Ena/VASP or filamentous actin in the front center of the cell (13,14).

The tight coupling of protrusion and retraction in coherent cells makes keratocytes an ideal model system for elucidating the manner in which events at the front of the cell

Submitted August 25, 2009, and accepted for publication October 30, 2009.

*Correspondence: theriot@stanford.edu

Editor: Douglas Nyle Robinson.

0006-3495/10/03/0933/10 $2.00

doi: 10.1016/j.bpj.2009.10.058

are coupled with events at the rear. In this work, we have observed keratocytes that, rather than gliding across the substrate, take small steps forward. In these cells, retraction of the trailing edge on one side of the cell body is out of phase with retraction on the other side, resulting in periodic lateral oscillation of the cell body. These oscillations are more prevalent in coherent keratocytes than in decoherent cells, suggesting that they may be the result of efficient integration of protrusive, contractile, and adhesion forces. We present experimental evidence to support a physical model for oscillation in which periodic retraction of the trailing edge is the result of elastic coupling with the leading edge.

METHODS

Cell culture and sample preparation

Keratocytes were cultured from the scales of the Central American cichlid *Hypsophrys nicaraguensis* as previously described (13). Briefly, scales were sandwiched between two acid-washed 25-mm glass coverslips and cultured at room temperature for 16–20 h using Leibovitz's L-15 medium (Gibco BRL, Carlsbad, CA) supplemented with 14.2 mM HEPES, pH 7.4, 10% FBS, and 1% antibiotic-antimycotic (Gibco BRL). Individual cells were obtained by disaggregating sheets of keratocytes with 2.5 mM EGTA in 85% PBS, pH 7.4, for 5–10 min. To facilitate tracking of the cell body, cells were loaded with the fluorescent volume marker CMFDA (Molecular Probes, Eugene, OR). Latrunculin A (Molecular Probes) or **GRGSS** peptides (Stanford PAN Facility, Stanford, CA) were added to cells in full media at a final concentration of 10 nM or 100 μg/ml, respectively. Cells were imaged 10–30 min after treatment.

Measurement of cell body and cell shape oscillations

Cells were imaged at 2- to 5-s intervals over 5–20 min, and the cell body centroid was determined by the weighted pixel intensity of the cell body. The path of the cell body was fit to a smooth curve generated by calculating the weighted moving average for each x and y coordinate, and the distance between the cell body centroid and the fit line was calculated at each time point. To measure edge velocities, cell outlines were extracted from phase images using Celltool, an open source collection of tools for quantifying cell shape, as described (13,23), and the velocity of the cell perimeter was calculated at evenly spaced points along the perimeter. The length of the cell on either side of the cell body from leading edge to trailing edge was measured in ImageJ. The frequencies of cell-body, cell-length, and edge-velocity oscillations were determined by fast Fourier transform. The significance of the measured frequency was assessed by determining the probability of getting the same peak in the power spectrum for randomly generated signals. Data analysis was performed using custom-written code in MATLAB 7 (The MathWorks, Natick, MA) and Python.

Model parameter choices

We estimated many of the parameter values for our model for keratocyte oscillations from measurements of keratocyte shape and speed. We chose $v_0 = 0.2$ μm/s, the average cell speed for a population of oscillating keratocytes, and $W = 20$ μm, the average cell width. Average cell length is ~15 μm, so we chose $L_0 = 10$ μm and $\bar{L}_0 = 5$ μm. To estimate v_1, v_2, α, and β, we measured the length of the cell, from leading edge to trailing edge, on either side of the cell body for four oscillating keratocytes that ranged in speed from 0.14 μm/s to 0.3 μm/s. The length of each cell on either side of the cell body oscillated in an anticorrelated, periodic fashion, as shown for one cell in Fig. 1 *D*, with an average $\Delta d = 2.5\mu$m. We resampled and averaged each cycle of retraction for each of the four cells and estimated the speed of the trailing edge as $v \approx v_0 - \dot{L}$ for an average cycle of retraction. Based on this, we estimated $v_1 \sim 0.08$ μm/s, $v_2 \sim 1$ μm/s, $\alpha \sim 0.5$ s, and $\beta \sim 25$ s. Motile keratocytes form adhesions to the substrate under the lamellipodium, but these adhesions are smaller than those formed at the trailing edge (19). Therefore, we assumed that γ, the friction coefficient at position $\bar{\mathbf{x}}$, was greater than α but less than β, and chose $\gamma = 4$ s. The elastic modulus of the lamellipodia of moving keratocytes, measured by atomic force microscopy (AFM), ranges between 10 kPa at the base of the lamellipodium, near the cell body, and 55 kPa at the leading edge (17). For a keratocyte with typical dimensions (20 μm wide, 15 μm long, and 200 nm high), this corresponds to a stiffness of ~3–15 nN/μm. However, the lamellipodium is so thin that AFM likely overestimates the elastic modulus due to the influence of the underlying, stiff glass substrate, and so we chose $K = 1$ nN/μm for the stiffness of the base of the lamellipodium and explored values for $\overline{K}$, the stiffness of the lamellipodium close to the leading edge, between 1 and 10 nN/μm. For K_w, the stiffness of the spring connecting $\mathbf{x_{21}}$ and $\mathbf{x_{2r}}$, we explored values between 0.1 and 100 nN/μm. Finally, we treated g, the memory term, as a free parameter and explored values between 0.01 and 10 s^2 nN/μm.

Model simulations

The dynamic equations for keratocyte motion (Eqs. 4–7) in the main text) were evaluated numerically in Mathematica with the parameter values discussed above. To determine the relative phase lag, ϕ, between the length oscillations for the left and right sides of the cell, we first calculated the period of oscillation, T, for both sides by fast Fourier transform. We then calculated the correlation coefficient, C, between the left side at time t and the right side at time $t + \mathrm{P}$ for $\mathrm{P} = 0$ to $\mathrm{P} = T$. ϕ was given by 1 - (P_{max}/T), where P_{max} is the value for P with the highest correlation coefficient. Simulated oscillations were classified as either in-phase ($0 < \phi < 0.1$) or antiphase ($0.4 < \phi < 0.5$), and either stable ($C > 0.8$) or irregular ($C < 0.8$). The correlation coefficient was defined as $C_{l,r} = \sum(l_i - \bar{l})(r_i - \bar{r})/(n-1)s_l s_r$, where $\bar{l}$ and $\bar{r}$ are the mean lengths and s_l and s_r are the standard deviations for the left and right sides of the cell, respectively. The sum was evaluated from $t = i - n$, where n is the number of time points.

RESULTS

By imaging moving keratocytes at high spatial and temporal resolution, we observed a common mode of migration for these cells in which retraction of the trailing edge on one side of the cell was out of phase with retraction on the other side (Fig. 1, *A* and *F–H*, and Movie S1, Movie S2, and Movie S3 in the Supporting Material). Antiphase retraction of the trailing edge resulted in periodic lateral oscillation of the cell body (Fig. 1, *A–C*). In addition, the length of the cell from leading edge to trailing edge on either side of the cell body oscillated, with the cell length on one side increasing and decreasing out of phase with the other side, with the same frequency as the lateral movement of the cell body (Fig. 1, *D* and *E*). Oscillations were confined to the rear of the cell; the leading edge moved forward with constant velocity (Fig. 1, *F–H*). We determined the prevalence of these oscillations by measuring the frequency of cell-body oscillation in a population of randomly selected cells ($n = 50$). Representative examples of oscillating and nonoscillating cells are shown in Fig. 2. Seventy-four percent of keratocytes oscillated with significant power, with periods ranging from 25 to 130 s and amplitudes between 0.5 and 3 μm for the lateral movement of the cell body.

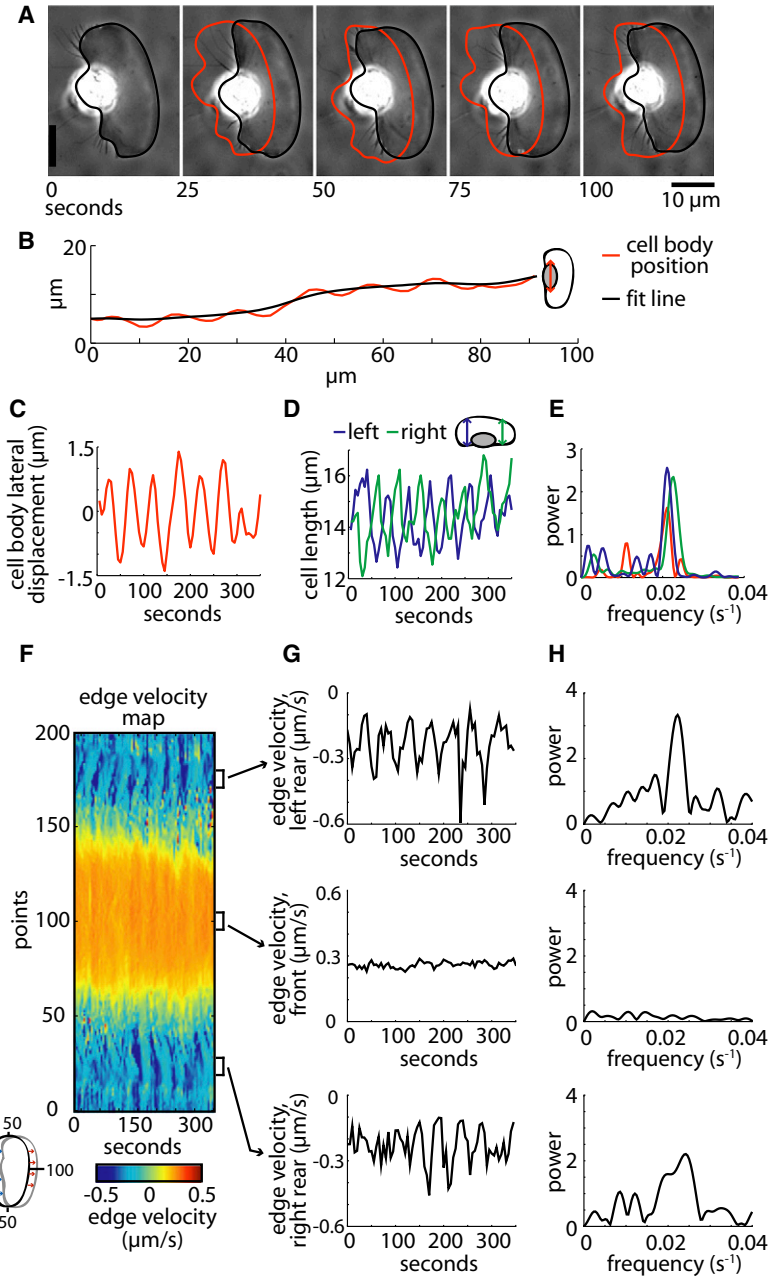

FIGURE 1 Periodic shape and movement oscillations. A locomoting keratocyte was imaged at 5-s intervals for 6 min, and the frequency of oscillation of cell body, cell length, and edge velocity were measured by fast Fourier transform. (*A*) Individual frames from the movie are shown at 25-s intervals; the outline of the cell from the preceding image is superimposed on each frame. Scale bar, 10 μm. (*B*) The position of the cell body centroid plotted in two dimensions (*red line*), fit to a smooth curve (*black line*). (*C*) Lateral displacement of the cell body. The distance between the cell body centroid and the fit line shown in *B* is plotted over time. (*D*) Cell length on the left (*blue line*) and right (*green line*) sides of the cell body over time. (*E*) Power spectra for cell body (*red line*) and cell length (*blue* and *green lines*) oscillations. The power of each transform is plotted versus frequency. (*F*) Edge velocity map. Cell outlines were extracted from each image and resampled such that point 0 is the cell rear and point 100 is the cell front. The velocity at each point on the cell perimeter is plotted over time. Negative velocities (*blue*) are retractions and positive values (*red*) are protrusions. (*G*) Velocities of the trailing edge to the left of the cell body (point 175; *upper graph*), the center of the leading edge (point 100; *middle graph*), and the trailing edge to the right of the cell body (point 25; *lower graph)* are plotted over time. (*H*) Power spectra for the velocities of the leading edge and trailing edge on either side of the cell body. The frequency of oscillation of the cell body, cell length, and trailing edge velocity for this cell is ~42 s.

Keratocytes range from coherent, fan-shaped, fast-moving cells with smooth leading edges, to decoherent, round, slow-moving cells with rough leading edges (13,14). To elucidate the difference between oscillating and nonoscillating cells, we measured cell speed, area, aspect ratio (the width of the cell perpendicular to the direction of motion divided by the length of the cell from leading edge to trailing edge), and leading-edge morphology (Fig. 2, *D–G*). Oscillating and nonoscillating cells were on average the same size (average cell area = 412 μm^2 and 430 μm^2, respectively (Fig. 2 *E*)), but oscillating cells were faster and more fan-shaped (average cell speed, 0.19 μm/s; average aspect ratio, 1.8) than nonoscillating cells (average cell speed, 0.09 μm/s, $p < 0.001$, Student's *t*-test; average aspect ratio, 1.6, $p < 0.05$, Fig. 2, *D* and *F*). To quantify leading-edge roughness, we measured local leading-edge curvature (13,14); cells with rough leading edges have high local curvature values and cells with smooth leading edges have low local curvature values. On average, oscillating cells had smoother leading edges (average local leading-edge curvature, 4.4) than nonoscillating cells (average local curvature, 8.0, $p < 0.005$, Fig. 2 *G*). Oscillating cells, then, were more coherent then nonoscillating cells, indicating that cell-body oscillation correlates with rapid cell movement and efficient front-to-back coordination.

We found that two possible candidates for contributing to retraction of the trailing edge—myosin and calcium

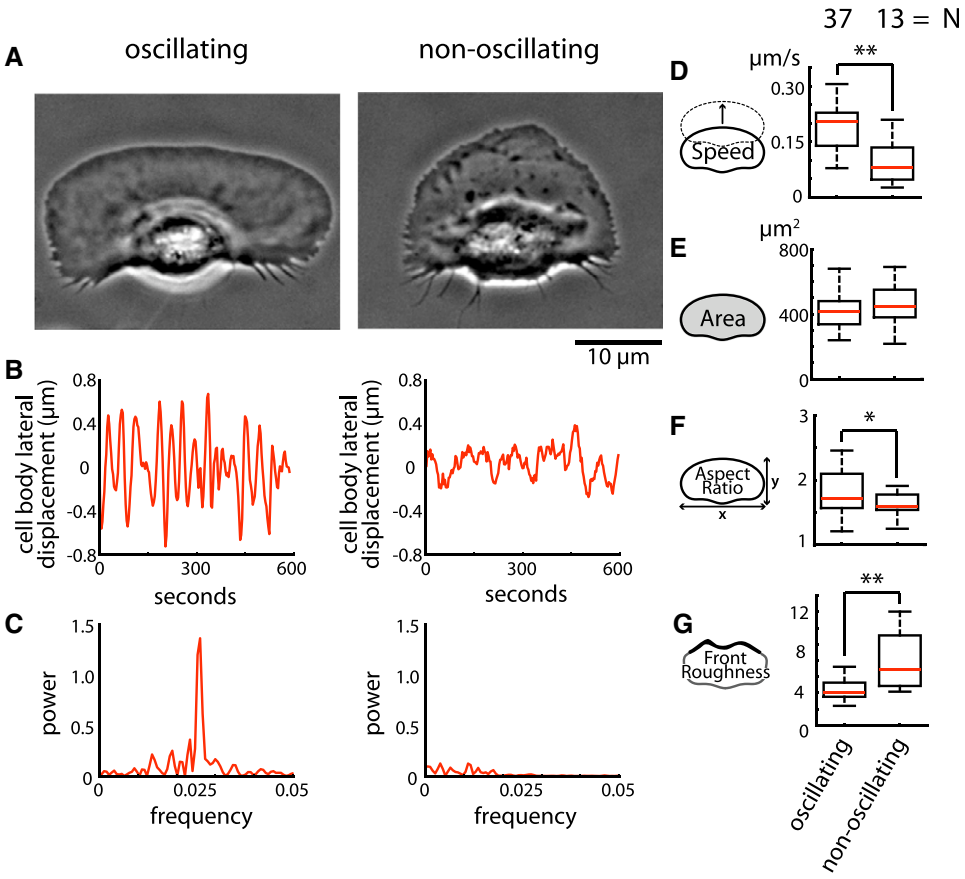

FIGURE 2 Oscillating cells are faster and more coherent than nonoscillating cells. A population of 50 randomly selected cells were imaged at 5-s intervals for 10 min, and the frequency of lateral cell body oscillation was measured by fast Fourier transform. Of the 50 cells, 37 oscillated with significant power (see Methods). (*A–C*) Representative examples of an oscillating cell (*right*) and a nonoscillating cell (*left*) are shown. (*A*) Phase images. (*B*) Lateral displacement of the cell body. The cell body position for each cell was fit to a smooth curve, and the distance between the fit line and the cell body position is plotted over time. (*C*) Power spectra for the cell body oscillations. (*D–G*) Box and whisker plots for cell speed (*D*), area (*E*), aspect ratio (*F*), and front roughness (*G*) for populations of oscillating and nonoscillating cells. The plots indicate the 25th percentile (*lower bound*), median (*red line*), 75th percentile (*upper bound*), and observations within 1.5 times the interquartile range (*whiskers*). Asterisks indicate significant differences between the oscillating and nonoscillating populations (*$p < 0.05$; **$p < 0.005$).

transients—were not required for keratocyte oscillation. Although Ca^{2+} transients have been shown to correlate with rear retraction in slow-moving, fibroblastlike keratocytes (24), Ca^{2+} transients observed in oscillating cells did not correlate with cell-body oscillation (Fig. S1, *A* and *B*), and inhibition of calcium transients did not abolish oscillation (Fig. S1 *C*). Inhibition of myosin II contraction with the small-molecule inhibitor blebbistatin (25) has been shown to abolish inward-directed actin network flow in the keratocyte rear (21) and in this study caused focal adhesions to shrink (Fig. S2) but did not inhibit oscillation or affect its frequency (Fig. S3). In keratocytes, myosin contraction exerts force on adhesion bonds perpendicular, rather than parallel, to the direction of migration (10), suggesting that adhesion strength and myosin contraction are normally balanced perpendicular to the direction of cell movement, and that elastic force parallel to the direction of motion is sufficient for oscillation.

We propose a model for keratocyte oscillation in which retraction of the trailing edge is the result of elastic coupling with the leading edge. It is known that cells are viscoelastic materials that display predominantly elastic behaviors over timescales up to tens of seconds (26,27), which is the relevant timescale for keratocyte migration. We have previously observed that keratocytes maintain the same shape over long time periods while migrating for tens or hundreds of cell diameters (14). This suggests that keratocytes can be treated as elastic bodies with preferred shapes such that any deformation from the default shape results in a restoring force. This general phenomenological description does not depend on the detailed nature of the elastic restoring force; multiple mechanical components of the cells may contribute, including the cytoskeleton and the rounded cell body. In an oscillating keratocyte, actin polymerization drives protrusion of the leading edge (4) and adhesions in the rear oppose retraction of the trailing edge (19). The front of the cell advances while the rear remains behind, cell length increases, and an elastic restoring force builds up. We assume that adhesions at the leading edge are much stronger than adhesions in the rear (19), and so when the elastic force generated by protrusion exceeds a critical force, adhesion bonds in the rear rupture, the trailing edge jumps forward, and the length of the cell decreases. As the trailing edge slows down again, adhesions reform, the cell stretches, and elastic forces increase until they again exceed the critical force where adhesions break, resulting in oscillations in cell length, as observed experimentally (Fig. 1 *D*).

We developed a quantitative model for keratocyte length oscillations, first in one dimension. In this simplified model, a moving cell has its front at position x_1 and its rear at position x_2, and the cell length is described by $L = x_1 - x_2$. The front of the cell moves forward with constant velocity,

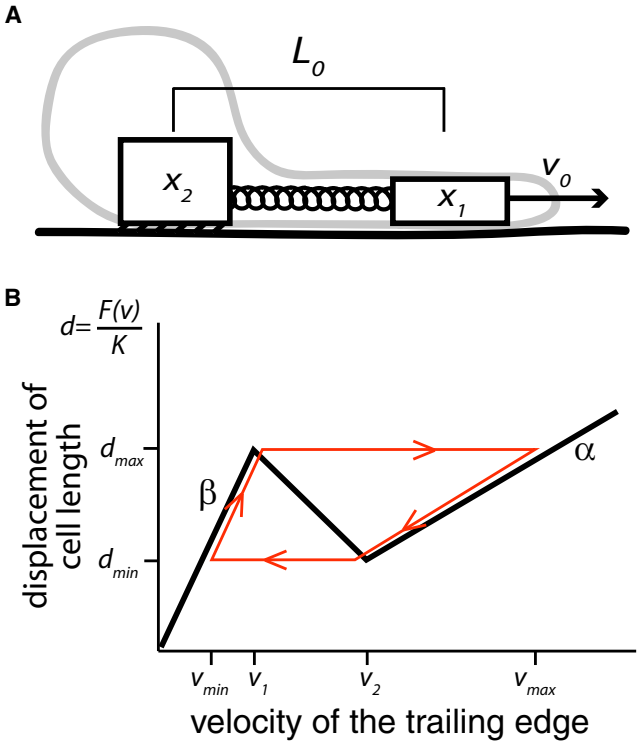

FIGURE 3 One-dimensional model for keratocyte oscillation. (*A*) The leading edge (position x_1) moves forward with constant velocity v_0. The trailing edge (position x_2) adheres to the substrate. The leading and trailing edges are connected by an elastic element with stiffness K and rest length L_0. (*B*) Schematic plot of d, the displacement of the cell length from rest, as a function of v, the velocity of the trailing edge. At small velocity, $v < v_1$, the rear of the cell forms adhesions to the substrate and moves more slowly than the front, and the cell stretches, with displacement $d = F(v)/K \approx \beta v$. When the speed of the trailing edge reaches v_1, the adhesions between the rear of the cell and substrate rupture, and v quickly increases to v_{max}. As the rear of the cell then begins to slow down, at large $v > v_2$ the length of the cell decreases with $d \approx \alpha v$. When $v < v_2$, adhesions reform between the cell and the substrate, the velocity of the rear slows to v_{min}, and the length of the cell again increases with $d \approx \beta v$.

$\dot{x}_1 = v_0$ (Fig. 3 *A*), driven by actin polymerization (4). The front of the cell is connected to the trailing edge by an elastic element with spring constant K and rest length L_0. The elastic force acting on the back from the front is $F_e = Kd$, where d is the displacement of the elastic element from its rest length: $d = x_1 - x_2 - L_0$. The rear of the cell adheres to the substrate, and as it slides along the substrate with velocity $\dot{x}_2 = v$, it exerts force on the substrate (10,11). For constant velocity, v, of the trailing edge, the adhesion force is a nonlinear function of v and thus an effective friction force: $F_a = F(v) = \lambda v$, where λ is a friction coefficient. The friction coefficient λ comes from the binding and detachment of adhesion bonds (28) (see Appendix) and cannot be easily measured. Therefore, we relate the friction coefficient λ in the system to the relaxation time $\tau = \lambda/K$ of the elastic element, which we can estimate from measured changes in L (see Methods). At small $v < v_1$, the rear of the cell forms adhesions to the substrate, and we approximate $F(v) \approx K\,\beta v$, where β is the relaxation time associated with cell adhesion. At larger velocity, $v > v_2$, the adhesions are broken, and we write $F(v) \approx K\,\alpha v$, where α is the relaxation time for nonspecific friction, which obeys $\alpha \ll \beta$. For $v_1 < v < v_2$, we estimate the unstable branch of the friction force as $F(v) = -K\,\beta v - \alpha v_2/v_2 - v_1(v - v_1) + K\beta v_1$ (Fig. 3 *B*). If velocity v changes in time, the friction force gradually changes via the kinetics of binding and detachment of adhesion molecules. This relaxation is captured by a coefficient, g, in the adhesion force: $F_a = F(v) + g\dot{v}$ (see Appendix). The dynamic equation for the position of x_2 results from the balance of elastic and adhesive forces, $F_e = F_a$, and reads

$$g\ddot{x}_2 = K(x_1 - x_2 - L_0) - F(\dot{x}_2). \quad (1)$$

In the limit where adhesion forces change instantaneously, $g = 0$, the period, T, of oscillation is given by

$$T = \beta \ln\left[1 + \frac{\Delta d}{\beta(v_0 - v_1)}\right] + \alpha \ln\left[1 + \frac{\Delta d}{\alpha(v_2 - v_0)}\right], \quad (2)$$

where $\Delta d = d_{max} - d_{min}$, and d_{max} and d_{min} are the maximum and minimum displacements, respectively, of the elastic element. The first term in this expression for the period T represents the rising phase, where the rear of the cell adheres to the substrate and cell length increases, and the second term represents the falling phase of the oscillation cycle, where adhesions in the rear are broken and cell length decreases. For simplicity, we assume that the rising phase is much longer than the falling phase, and approximate T as

$$T \approx \frac{\Delta d}{(v_0 - v_1)}. \quad (3)$$

We estimated parameter values for this model from measurements of keratocyte shape and speed (see Methods). Values for T calculated with these parameter values using either Eq. 2 or Eq. 3 were within 15% of each other, which is comparable to the variability in the experimental data. Thus, Eq. 3 is a reasonable approximation of Eq. 2 for the keratocyte system.

This simple one-dimensional model makes a number of specific quantitative predictions about the behavior of oscillating keratocytes. First, if elastic force generated by protrusion of the leading edge causes retraction of the trailing edge, then the faster a cell moves, the faster the elastic force reaches the critical force, and the higher the frequency of oscillation (see Eq. 3). The frequency of oscillation should therefore correlate with v_0. To test this, we measured cell-speed and cell-body oscillation in a large population of cells ($n = 98$), and the frequency of oscillation did in fact correlate with the speed of the cell (Fig. 4 *A*). Moreover, by rewriting Eq. 3 as $v_0 = f\Delta d + v_1$, where the frequency of oscillation is $f = 1/T$, we can see that the slope of the fit line in Fig. 4 *A* is approximately equal to Δd, the change in cell length in one oscillation cycle, and the y intercept is equal to v_1, the critical velocity where adhesions in the rear rupture. The Δd

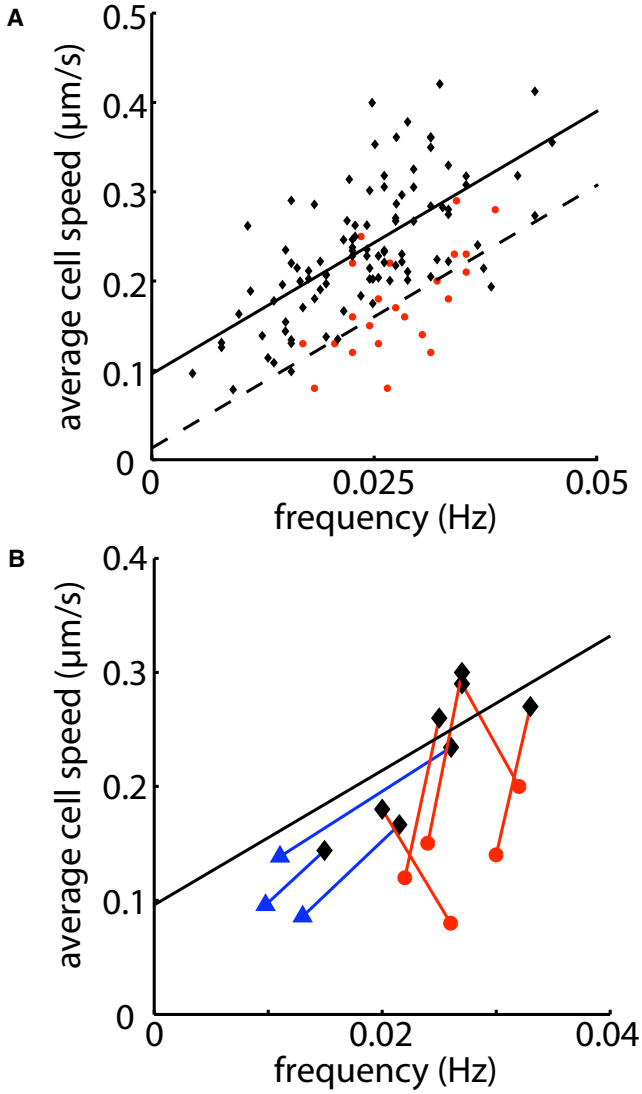

FIGURE 4 Cell body oscillation correlates with cell speed. (*A*) The frequency of oscillation for a population of control cells (*black diamonds*, $n = 98$) and cells treated with 100 μg/ml RGD (*red circles*, $n = 23$) was measured by fast Fourier transform and is plotted versus cell speed. Cell speed significantly correlates with frequency of oscillation for both control (*solid line*, $R^2 = 0.44$, $p < 0.01$) and RGD-treated cells (*dashed line*, $R^2 = 0.3$, $p = 0.01$), with the RGD-treated cells oscillating at higher frequencies at relatively lower speeds. To determine whether the two populations were significantly different, we compared the residuals from the control fit line for both the control and RGD-treated populations; the mean residual value for the RGD population (-0.08 ± 0.01) was significantly different from the mean residual for the control population (0 ± 0.006, $p < 10^{-9}$, Student's *t*-test). (*B*) Oscillation frequency for individual cells is plotted versus cell speed before (*black diamonds*) and after treatment with either 10 nM latrunculin A (*blue triangles*) or 100 μg/ml RGD peptides (*red circles*). The solid black line is the fit line from the control population in *A*.

calculated using this argument for a population of keratocytes (~5 μm) is comparable to that measured for individual keratocytes (Fig. 1 *D*).

Second, the model predicts that for oscillations to occur, cell speed v_0 must be greater than the critical rupture velocity, v_1. Consistent with this prediction, the value for v_1 calculated from the fit line in Fig. 3 *A* (0.10 μm/s) is less than the average cell speed of oscillating keratocytes (0.19 μm/s) but greater than the average speed of nonoscillating keratocytes (0.09 μm/s (Fig. 2 *D*)). It may be, then, that decoherent cells do not oscillate because they move too slowly; in these cells, the elastic force never exceeds the critical rupture force, and so, rather than simply breaking, adhesions in the rear must disassemble via more complicated mechanisms. Consistent with this, we have observed that whereas adhesions in the rear of coherent, oscillating keratocytes rupture as the trailing edge retracts, adhesions in the rear of decoherent, nonoscillating cells slide inward and disassemble as the trailing edge moves forward (Fig. S4, Movie S4, and Movie S5).

Third, the model predicts that disrupting adhesion should reduce the elastic force required for retraction, and v_1 should decrease. At any given v_0, as v_1 decreases, the period of oscillation should also decrease (see Eq. 3). To test this, we treated a population of keratocytes with Arg-Gly-Asp (RGD) peptides. Adhesion of cells to the extracellular matrix is mediated by integrin binding to RGD motifs in extracellular matrix proteins (29,30). Soluble RGD peptides have been shown to inhibit adhesion in fibroblasts by competing with substrate ligands for integrin binding sites (30), and global addition of high concentrations of RGD peptides to keratocytes causes them to round up (Fig. S5), suggesting that RGD peptides also inhibit keratocyte adhesion. As predicted by the model, inhibition of adhesion with a low concentration of RGD peptides (100 μg/ml) affected the relationship between frequency of oscillation and cell speed. Cells treated with RGD continued to oscillate, but with higher frequencies of oscillation at the same or even lower speeds compared to control cells (Fig. 4 *B*), and the measured value for v_1 was significantly lower (0.02 μm/s) than that for control cells (0.10 μm/s) (Fig. 4 *A*). In contrast, inhibiting actin polymerization with a low dose of latrunculin A, and thereby slowing protrusion, decreased the frequency of oscillation (Fig. 4 *B*), consistent with the prediction that the speed of the cell dictates the frequency of oscillation rather than vice versa.

This simple one-dimensional stick/slip model nicely describes much of our data, but cannot account for the observation that retraction of the trailing edge on one side of the cell occurs out of phase with retraction on the other side. We describe these antiphase retractions with a more realistic two-dimensional model. In the two-dimensional model, we incorporate the observation that motile keratocytes have adhesions on either side of the cell body (19,22), so the rear of the cell can be separated into a left and a right side with positions $\mathbf{x_{2l}}$ and $\mathbf{x_{2r}}$ (Fig. 5 *A*). Each side adheres separately and is attached to an elastic element with modulus K and rest length L_0. These elastic elements are connected to the front of the cell, denoted $\mathbf{x_l}$ as before, at position $\overline{\mathbf{x}}$ by an elastic element with modulus $\overline{K}$ with rest length $\overline{L}_0$. In addition, $\mathbf{x_{2l}}$ and $\mathbf{x_{2r}}$ are connected to each other by an

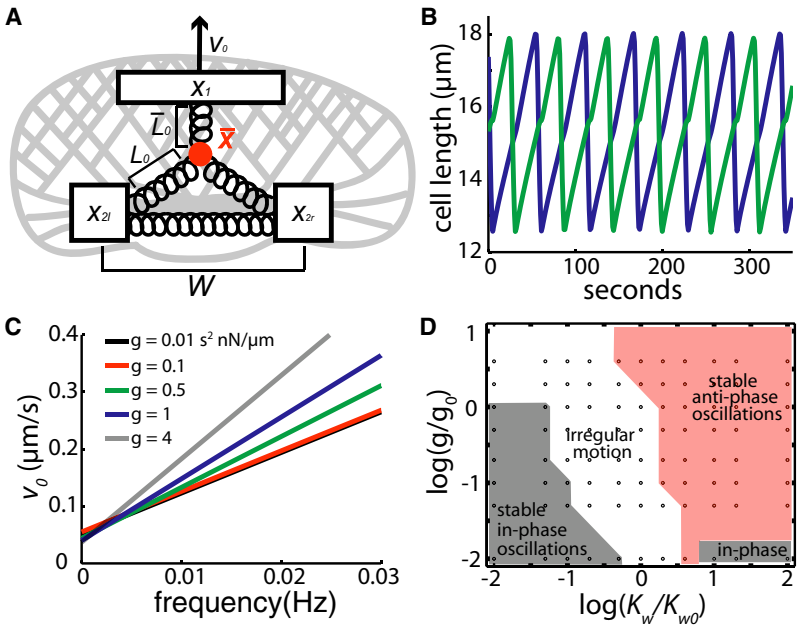

FIGURE 5 Two-dimensional model. (*A*) The leading edge is connected to the trailing edge (positions $\mathbf{x_{2l}}$ and $\mathbf{x_{2r}}$) by springs $\overline{K}$ and K, which have rest lengths $\overline{L}_0$ and L_0, respectively. $\mathbf{x_{2l}}$ and $\mathbf{x_{2r}}$ are connected to each other by spring K_w, with rest length W. (*B*) Simulated cell length (distance between $\mathbf{x_l}$ and $\mathbf{x_{2l}}$ or $\mathbf{x_{2r}}$) oscillations for $v_0 = 0.2$ μm/s, shown for both left (*blue*) and right (*green*) sides. (*C*) The frequency of oscillation correlates with v_0 for a wide range of values for g. (*D*) State diagram of cell length oscillations. Equations 4–7 were evaluated numerically at the indicated values for g and K_w (*circles*). To determine whether the oscillations were stable or irregular, the time correlation coefficient, C, was calculated between the left, $L(t)$, and right, $R(t + P)$ sides, where P is the time lag between the two sides (see Methods). Oscillations were defined as stable antiphase (*pink shading*), with relative phase lag between 0.4 and 0.5, and $C > 0.8$; stable in-phase (*gray shading*), with relative phase lag between 0 and 0.1, and $C > 0.8$; and having irregular motion (*no shading*), defined as $C < 0.8$. $g_0 = 1$ s^2 nN/μm; $K_{w0} = 1$ nN/μm. Parameter values used in *B–D* are $W = 20$ μm, $L_0 = 10$ μm, $\overline{L}_0 = 5$ μm, $v_1 = 0.08$ μm/s, $v_2 = 1$ μm/s, $\alpha = 0.5$ s, $\beta = 25$ s, $\gamma = 4$ s, $K = 1$ nN/μm, $\overline{K} = 10$ nN/μm, $K_w = 10$ nN/μm, and $g = 0.1$ s^2 nN/μm.rrruu.

additional element with stiffness K_w and rest length W. To find the positions $\mathbf{x_l}$, $\overline{\mathbf{x}}$, $\mathbf{x_{2l}}$, and $\mathbf{x_{2r}}$, we first define the unit vector pointing in the direction of motion, $\mathbf{n} = \mathbf{x}_1 - \overline{\mathbf{x}}/|\mathbf{x}_1 - \overline{\mathbf{x}}|$, and the three unit vectors $\mathbf{n_r} = \overline{\mathbf{x}} - \mathbf{x_{2r}}/|\overline{\mathbf{x}} - \mathbf{x_{2r}}|$, $\mathbf{n_l} = \overline{\mathbf{x}} - \mathbf{x_{2l}}/|\overline{\mathbf{x}} - \mathbf{x_{2l}}|$, and $\mathbf{n_w} = \mathbf{x_{2r}} - \mathbf{x_{2l}}/|\mathbf{x_{2r}} - \mathbf{x_{2l}}|$. The position of the leading edge is given by

$$\dot{\mathbf{x}}_\mathbf{1} = v_0\mathbf{n}. \tag{4}$$

The dynamic equations for $\mathbf{x_{2l}}$ and $\mathbf{x_{2r}}$ again result from the balance of elastic and adhesive forces, with an additional elastic force that comes from one side of the cell acting on the other side:

$$g\ddot{\mathbf{x}}_{2\mathbf{r}} = \mathbf{n_r}K(|\overline{\mathbf{x}} - \mathbf{x_{2r}}| - L_0) - \frac{\dot{\mathbf{x}}_{2\mathbf{r}}}{|\dot{\mathbf{x}}_{2\mathbf{r}}|}F(|\dot{\mathbf{x}}_{2\mathbf{r}}|) - \mathbf{n}_w K_w(|\mathbf{x_{2r}} - \mathbf{x_{2l}}| - W); \tag{5}$$

$$g\ddot{\mathbf{x}}_{2\mathbf{l}} = \mathbf{n_l}K(|\overline{\mathbf{x}} - \mathbf{x_{2l}}| - L_0) - \frac{\dot{\mathbf{x}}_{2\mathbf{l}}}{|\dot{\mathbf{x}}_{2\mathbf{l}}|}F(|\dot{\mathbf{x}}_{2\mathbf{l}}|) + \mathbf{n}_w K_w(|\mathbf{x_{2r}} - \mathbf{x_{2l}}| - W). \tag{6}$$

The position of $\overline{\mathbf{x}}$ is determined by the balance of elastic forces and an additional friction with coefficient γ:

$$\gamma\frac{d\overline{\mathbf{x}}}{dt} = \mathbf{n}\overline{K}(|\mathbf{x_1} - \overline{\mathbf{x}}| - \overline{L}_0) - \mathbf{n_r}K(|\overline{\mathbf{x}} - \mathbf{x_{2r}}| - L_0) - \mathbf{n_l}K(|\overline{\mathbf{x}} - \mathbf{x_{2l}}| - L_0). \tag{7}$$

We solved Eqs. 4–7 numerically (see Methods for a discussion of parameter choices). An example of spontaneous oscillations in cell length is shown in Fig. 5 *B*. The length of the left and right sides of the system oscillate in antiphase, with a frequency and amplitude consistent with that measured for keratocytes, and the linear relationship between cell speed and frequency of oscillation was preserved (Fig. 4 *C*). In general, we found that stable, antiphase oscillations occur at $K_w > 2$ nN/μm for various values of g; for lower values of K_w, oscillations are either stable and in phase, or motion is irregular (Fig. 5 *D*). In addition, we found that antiphase oscillations occur for all values of $\overline{K}$ between 1 and 10 nN/μm, although larger values of $\overline{K}$ resulted in a higher frequency of oscillation and a smaller average cell length. AFM measurements of keratocytes gave estimated values for lamellipodial stiffness on the order of 3–15 nN/μm (17), consistent with our observations of stable antiphase oscillations for most cells.

DISCUSSION

Motile keratocytes are dynamic systems in which interactions among several elements—including the actin-based protrusion machinery, an elastic cell body, and adhesions in the rear—give rise to oscillations. We have presented experimental evidence to support a model for oscillation in which force from adhesions in the rear balances the elastic force generated by protrusion: adhesions rupture when the elastic force exceeds a critical threshold, resulting in oscillations in cell length. Spontaneous oscillations of cytoskeletal structures have been observed in other systems, including positional oscillation of the posterior spindle pole during asymmetric division of the *Caenorhabditis elegans* egg (31) and oscillations in speed for actin-based motility in ''hopping'' *Listeria monocytogenes* (32,33). Taken together, our results and theoretical descriptions of spindle-pole oscillations (34) and *Listeria* ''hopping'' (35,36), suggest that

oscillations may be a general characteristic of force-generating systems that act on elastic elements (37).

What is the relevant elastic element in oscillating keratocytes? Our model for keratocyte oscillation depends on the assumption that keratocytes can be treated as elastic bodies with preferred shapes. This assumption is consistent with experimental evidence that cells are predominantly elastic over timescales relevant for keratocyte oscillation (26) and with the previous observation that migrating keratocytes maintain the same shape over long periods of time (14). However, unlike spindle-pole oscillations and Listeria ''hopping'', where microtubules or an actin comet tail, respectively, determine the elastic properties of the system, it is unlikely that a single element determines the elastic properties of the keratocyte. The mechanical properties of cells are complex, and multiple components, such as the cross-linked actin network, microtubules, and intermediate filaments, as well as the cell membrane, the elastic nucleus, and the cytoplasm itself, contribute to the elastic modulus (25). Moreover, these elements are out-of-equilibrium, highly dynamic structures: the cytoskeletal filaments polymerize and depolymerize and, in addition, are organized by dynamic cross-linkers and molecular motors, and the plasma membrane is recycled through internal stores via endocytosis and exocytosis. Thus, the connection between the leading and trailing edges in a crawling cell is an active elastic system that is composed of many elements, rather than a simple passive spring. The manner in which specific elements contribute to the behavior of active elastic systems is not well understood, particularly for systems as complex as a crawling cell. Further experiments, in both in vitro systems and relatively simple cells like the keratocyte, along with further theoretical work, will be required to tease apart the contributions of specific elements to cell elasticity and behavior.

Although the majority of keratocytes oscillate, we found that ~25% of keratocytes do not oscillate with detectable amplitude. Keratocytes that do not oscillate tend to be more decoherent—they are slower and less well-organized—than oscillating keratocytes. Our model is applicable to both the coherent oscillating and decoherent nonoscillating populations, since it identifies criteria required for oscillation. First, according to the one-dimensional model, for a cell to oscillate, the speed of the cell, v_0, must be greater than the critical speed at which adhesions in the rear rupture, v_1 (estimated to be 0.10 μm/s). We have shown that cells that do not oscillate migrate at speeds lower than the critical rupture velocity estimated from our population-based measurements. It may be, then, that cells that do not oscillate simply move too slowly for adhesions in the rear to rupture; instead, adhesions in these cells are remodeled by slower turnover mechanisms (Fig. S4). Second, numerical analysis of our two-dimensional model showed that a stiff cell body is required for stable antiphase oscillations. In addition to being too slow, decoherent cells may be too compliant for information about the movement of the leading edge to be reliably communicated to the trailing edge via stretching of the cell. In principle, it should be possible to measure the stiffness of oscillating and nonoscillating cells to see whether the stiffness of the cell correlates with oscillation.

Keratocyte morphology is different from that of most other well characterized motile cell types, such as *Dictyostelium*, leukocytes, and fibroblasts. However, each of these cell types depends on the same machinery—a branched, elastic actin network, dynamic adhesions, and, to varying degrees, myosin contraction—for migration, and oscillations in cell shape and speed have been observed in *Dictyostelium* (38) and leukocytes (39). Recent top-down modeling of cell migration suggests that differences in motile cell morphology can be the result of quantitative changes in a set of conserved control parameters such as protrusion and retraction rates and adhesion assembly rates and half-lives (40). Our model for keratocyte oscillation may therefore be relevant for other motile, oscillating cells. In keratocytes, because adhesions are separated into two clusters on either side of the cell body (19,22), when adhesions break on one side of the cell, the keratocyte is still able to effectively keep one foot on the ground, allowing it to maintain constant speed. In cells such as leukocytes, however, adhesions are often localized to one large cluster in the rear of the cell (41), and so rupture of adhesions in the rear would be expected to result in oscillations of cell body speed in addition to oscillations in cell length. Consistent with the general applicability of our model, measurement of oscillations in cell length and traction force generation in *Dictyostelium* have shown that the frequency of oscillation correlates with cell speed, even in mutants that lack myosin II (38), suggesting that elastic coupling between the front and back of the cell may be responsible for oscillations in *Dictyostelium* as well as in keratocytes. On the whole, simple elastic coupling between leading-edge protrusion and rear retraction appears to represent a mechanical mechanism for signal transduction, where information about events at the front of the cell is rapidly and reliably communicated to structures at the rear, with no apparent requirement for diffusible chemical messengers (42). Such mechanical communication may play a significant role in the large-scale organization of dynamic cells and tissues.

APPENDIX

Memory term in adhesion forces

We describe the force associated with adhesion molecules on the substrate as a friction force, F_a. F_a depends on the velocity, v, between the trailing edge of the cell and substrate, which we first consider to be constant. If $\overline{N}_b$ adhesion bonds with elastic stiffness k and lifetime $1/\omega_{off}$ are attached, the effective friction force is $F_a = \lambda v$, where the friction coefficient is $\lambda \approx \overline{N}_b k/\omega_{off}$. If bonds form with a rate ω_{on} and dissociate with a rate ω_{off}, then $\overline{N}_b = N\omega_{on}/(\omega_{on} + \omega_{off})$, where N denotes the number of available adhesion molecules. In general, since adhesion bond rupture depends

on the force that acts on the bond (43), the detachment rate, $\omega_{off} \approx \omega_0 \exp(|f|/f_c)$, where the critical force is $f_c = k_B T/a$ and a is a molecular length. This force-dependent rupture leads to the nonlinear friction described in the main text. If we now consider the case where the velocity, v, changes in t, the number of adhesion bonds, N_b, also changes. Considering the dynamics of bond formation and rupture, $\dot{N}_b = -\omega_{off} + \omega_{on}(N - N_b)$, we find that N_b relaxes to the stationary value as $N_b = \overline{N}_b + \delta N e^{-t/\tau}$, where $\tau = (\omega_{on} + \omega_{off})^{-1}$ is a relaxation time. This implies that the friction force also relaxes on this timescale. This relaxation of the friction force can be captured by an additional term in the friction, $F_a \approx \lambda v + g\dot{v}$, where $\tau = g/\lambda$. This expression is valid for slow velocity changes. We thus estimate that $g = \overline{N}_b k/[\omega_{off}(\omega_{on} + \omega_{off})]$.

SUPPORTING MATERIAL

Five figures and five movies are available at http://www.biophysj.org/biophysj/supplemental/S0006-3495(09)06003-2.

We acknowledge C. A. Wilson for the initial observation of keratocyte oscillation. We thank K. Keren for many helpful discussions, and E. Espinosa, N. Dye, and K. Keren for critical reading of the manuscript.

E.L.B. was supported by the National Institute of General Medical Sciences. G.M.A was supported by the Medical Scientist Training Program. J.A.T. was supported by the American Heart Association.

REFERENCES

1. Lauffenburger, D. A., and A. F. Horwitz. 1996. Cell migration: a physically integrated molecular process. *Cell*. 84:359–369.
2. Keren, K., and J. Theriot. 2008. Biophysical aspects of actin-based cell motility in fish epithelial keratocytes. *In* Cell Motility. P. Lenz, editor. Springer, New York. 31–58.
3. Gupton, S. L., and C. M. Waterman-Storer. 2006. Spatiotemporal feedback between actomyosin and focal-adhesion systems optimizes rapid cell migration. *Cell*. 125:1361–1374.
4. Theriot, J. A., and T. J. Mitchison. 1991. Actin microfilament dynamics in locomoting cells. *Nature*. 352:126–131.
5. Pollard, T. D., and G. G. Borisy. 2003. Cellular motility driven by assembly and disassembly of actin filaments. *Cell*. 112:453–465.
6. Mogilner, A., and G. Oster. 1996. Cell motility driven by actin polymerization. *Biophys. J*. 71:3030–3045.
7. Jay, P. Y., P. A. Pham, …, E. L. Elson. 1995. A mechanical function of myosin II in cell motility. *J. Cell Sci*. 108:387–393.
8. DiMilla, P. A., K. Barbee, and D. A. Lauffenburger. 1991. Mathematical model for the effects of adhesion and mechanics on cell migration speed. *Biophys. J*. 60:15–37.
9. Balaban, N. Q., U. S. Schwarz, …, B. Geiger. 2001. Force and focal adhesion assembly: a close relationship studied using elastic micropatterned substrates. *Nat. Cell Biol*. 3:466–472.
10. Lee, J., M. Leonard, …, K. Jacobson. 1994. Traction forces generated by locomoting keratocytes. *J. Cell Biol*. 127:1957–1964.
11. Oliver, T., M. Dembo, and K. Jacobson. 1995. Traction forces in locomoting cells. *Cell Motil. Cytoskeleton*. 31:225–240.
12. Goodrich, H. 1924. Cell behavior in tissue cultures. *Biol. Bull*. 46:252–262.
13. Lacayo, C. I., Z. Pincus, …, J. A. Theriot. 2007. Emergence of large-scale cell morphology and movement from local actin filament growth dynamics. *PLoS Biol*. 5:e233.
14. Keren, K., Z. Pincus, …, J. A. Theriot. 2008. Mechanism of shape determination in motile cells. *Nature*. 453:475–480.
15. Ream, R. A., J. A. Theriot, and G. N. Somero. 2003. Influences of thermal acclimation and acute temperature change on the motility of epithelial wound-healing cells (keratocytes) of tropical, temperate and Antarctic fish. *J. Exp. Biol*. 206:4539–4551.
16. Svitkina, T. M., A. B. Verkhovsky, …, G. G. Borisy. 1997. Analysis of the actin-myosin II system in fish epidermal keratocytes: mechanism of cell body translocation. *J. Cell Biol*. 139:397–415.
17. Laurent, V. M., S. Kasas, …, J. J. Meister. 2005. Gradient of rigidity in the lamellipodia of migrating cells revealed by atomic force microscopy. *Biophys. J*. 89:667–675.
18. Vallotton, P., G. Danuser, …, A. B. Verkhovsky. 2005. Tracking retrograde flow in keratocytes: news from the front. *Mol. Biol. Cell*. 16:1223–1231.
19. Lee, J., and K. Jacobson. 1997. The composition and dynamics of cell-substratum adhesions in locomoting fish keratocytes. *J. Cell Sci*. 110:2833–2844.
20. Bohnet, S., R. Ananthakrishnan, …, A. B. Verkhovsky. 2006. Weak force stalls protrusion at the leading edge of the lamellipodium. *Biophys. J*. 90:1810–1820.
21. Schaub, S., S. Bohnet, …, A. B. Verkhovsky. 2007. Comparative maps of motion and assembly of filamentous actin and myosin II in migrating cells. *Mol. Biol. Cell*. 18:3723–3732.
22. Anderson, K. I., and R. Cross. 2000. Contact dynamics during keratocyte motility. *Curr. Biol*. 10:253–260.
23. Pincus, Z., and J. A. Theriot. 2007. Comparison of quantitative methods for cell-shape analysis. *J. Microsc*. 227:140–156.
24. Lee, J., A. Ishihara, …, K. Jacobson. 1999. Regulation of cell movement is mediated by stretch-activated calcium channels. *Nature*. 400:382–386.
25. Straight, A. F., A. Cheung, …, T. J. Mitchison. 2003. Dissecting temporal and spatial control of cytokinesis with a myosin II inhibitor. *Science*. 299:1743–1747.
26. Kasza, K. E., A. C. Rowat, …, D. A. Weitz. 2007. The cell as a material. *Curr. Opin. Cell Biol*. 19:101–107.
27. Kruse, K., J. F. Joanny, …, J. Prost. 2006. Contractility and retrograde flow in lamellipodium motion. *Phys. Biol*. 3:130–137.
28. Filippov, A. E., J. Klafter, and M. Urbakh. 2004. Friction through dynamical formation and rupture of molecular bonds. *Phys. Rev. Lett*. 92:135503.
29. Pierschbacher, M. D., and E. Ruoslahti. 1984. Cell attachment activity of fibronectin can be duplicated by small synthetic fragments of the molecule. *Nature*. 309:30–33.
30. Ruoslahti, E. 1996. RGD and other recognition sequences for integrins. *Annu. Rev. Cell Dev. Biol*. 12:697–715.
31. Grill, S. W., P. Gönczy, …, A. A. Hyman. 2001. Polarity controls forces governing asymmetric spindle positioning in the *Caenorhabditis elegans* embryo. *Nature*. 409:630–633.
32. Lasa, I., E. Gouin, …, P. Cossart. 1997. Identification of two regions in the N-terminal domain of ActA involved in the actin comet tail formation by *Listeria monocytogenes*. *EMBO J*. 16:1531–1540.
33. Soo, F. S., and J. A. Theriot. 2005. Large-scale quantitative analysis of sources of variation in the actin polymerization-based movement of *Listeria monocytogenes*. *Biophys. J*. 89:703–723.
34. Grill, S. W., K. Kruse, and F. Jülicher. 2005. Theory of mitotic spindle oscillations. *Phys. Rev. Lett*. 94:108104.
35. Gerbal, F., P. Chaikin, …, J. Prost. 2000. An elastic analysis of *Listeria monocytogenes* propulsion. *Biophys. J*. 79:2259–2275.
36. Bernheim-Groswasser, A., J. Prost, and C. Sykes. 2005. Mechanism of actin-based motility: a dynamic state diagram. *Biophys. J*. 89:1411–1419.
37. Kruse, K., and F. Jülicher. 2005. Oscillations in cell biology. *Curr. Opin. Cell Biol*. 17:20–26.
38. Del Alamo, J. C., R. Meili, …, J. C. Lasheras. 2007. Spatio-temporal analysis of eukaryotic cell motility by improved force cytometry. *Proc. Natl. Acad. Sci. USA*. 104:13343–13348.

39. Hartman, R. S., K. Lau, …, T. D. Coates. 1994. The fundamental motor of the human neutrophil is not random: evidence for local non-Markov movement in neutrophils. *Biophys. J.* 67:2535–2545.

40. Satulovsky, J., R. Lui, and Y. L. Wang. 2008. Exploring the control circuit of cell migration by mathematical modeling. *Biophys. J.* 94:3671–3683.

41. Campanero, M. R., P. Sánchez-Mateos, …, F. Sánchez-Madrid. 1994. ICAM-3 regulates lymphocyte morphology and integrin-mediated T cell interaction with endothelial cell and extracellular matrix ligands. *J. Cell Biol.* 127:867–878.

42. Na, S., O. Collin, …, N. Wang. 2008. Rapid signal transduction in living cells is a unique feature of mechanotransduction. *Proc. Natl. Acad. Sci. USA*. 105:6626–6631.

43. Bell, G. I. 1978. Models for the specific adhesion of cells to cells. *Science*. 200:618–627.